Immobilisation of TiO_2 films on activated carbon fibres by a hydrothermal method for photocatalytic degradation of toluene

Peng Liang ✉, *Aifang Wei, Yaqing Zhang, Jiafeng Wu, Xiwang Zhang, Shufang Li*

Environmental and Chemical Engineering College, Shandong University of Science and Technology, Shandong, Qingdao, People's Republic of China
✉ *E-mail: liangpeng202@hotmail.com*

Published in Micro & Nano Letters; Received on 6th April 2016; Revised on 9th June 2016; Accepted on 13th June 2016

To improve the degradation efficiency of TiO_2 for low concentrations of volatile organic compounds, TiO_2 loaded on activated carbon fibres (ACF) was prepared by an impregnation–hydrothermal method. The crystal structure, surface area, dispersion, optical absorption properties, and chemical composition of the TiO_2/ACF composite materials were characterised by X-ray diffraction, Brunauer–Emmett–Teller analysis, scanning electron microscopy, ultraviolet–visible absorption spectroscopy, and X-ray photoelectron spectroscopy. The influence of the hydrothermal temperature, illumination time, space velocity, and light intensity on the photocatalytic activities of the TiO_2/ACF composite materials was investigated with toluene as a model pollutant. The results showed that the phase of TiO_2 was anatase, which was dispersed as a thin film on the ACF surface. The crystallinity, dispersion, UV absorption, and hydroxyl group content of TiO_2 increased with an increase of hydrothermal temperature, whereas the photocatalytic activity of TiO_2/ACF was maximised when the hydrothermal temperature was 180°C. Increases in illumination time, space velocity, and light intensity were beneficial for regeneration of the composite materials. However, the energy efficiency decreased with increased light intensity. The degradation efficiency of toluene reached 40% with reaction conditions of illumination time: 3 h, space velocity: 1400 h^{-1}, and light intensity: 32 W. This degradation efficiency decreased 3.3% after recycling five times.

1. Introduction: Recently, the consumption of indoor decoration materials has increased significantly owing to enhanced living standards. Many decoration materials contain volatile organic compounds (VOCs), which are a major contributor to indoor air pollution. Among VOCs, toluene is a typical pollutant, which has toxicity and carcinogenic potential. Long-term exposure to toluene will cause serious harm to human health. Photocatalytic technology has attracted increasing attention in the field of indoor air purification because it can non-selectively and completely mineralise VOCs into CO_2 and H_2O [1]. The most commonly used photocatalysts are ZnO, Fe_2O_3, TiO_2, and CdS [2], among which TiO_2 has the advantages of high stability, high activity, and low price [3]. However, because the concentration of VOCs in indoor air is relatively low, the contact time between VOCs and the photocatalyst is very short, which causes low photocatalytic degradation efficiencies [4]. This has hindered the application of photocatalysts for indoor air purification. An effective strategy to overcome this shortcoming is to use TiO_2 supported on activated carbon fibres (ACF). ACF has a well-developed pore structure and large specific surface area, which can not only improve the photocatalytic properties of TiO_2, but also realise the in situ regeneration of ACF [5]. Several methods have been developed to immobilise TiO_2 on ACF, such as the bonding process, the sol–gel method, electrostatic spinning, dip-coating, and the hydrothermal method. Yuan *et al.* [6] prepared TiO_2-loaded ACF with epoxy resin as a binder and showed that increasing pore size can improve the photocatalytic activity. Guo [7] prepares activated carbon supported TiO_2 by a sol–gel method and studied the degradation efficiency of phenol, which could be controlled by the heat treatment temperature, TiO_2 loading, catalyst dosage, and other factors. Wu *et al.* [8] prepared TiO_2/ACF nanofibres by an electrospinning method and reported that the preoxidation temperature has a decisive effect on the properties of the carbon fibres. Zhong *et al.* [9] coated TiO_2 onto glass fibres and carbon fibres and investigated their adsorption capacities for nine kinds of VOCs. They found that the adsorption behaviour is highly dependent on the substrate. In contrast with these methods, the hydrothermal method is well known to be a more promising method because it can be used to directly synthesise high purity anatase TiO_2 with a narrow particle size distribution. Shi *et al.* [10] suggested that the hydrothermal method could improve the combination of ACF and TiO_2 to achieve higher catalytic activity than that obtained using the coating method. Wang *et al.* [11] deposited three-dimensional TiO_2 flower-like structures on the surface of ACF by a hydrothermal method and showed that the activity of TiO_2/ACF was significantly higher than that of rutile TiO_2. Meng *et al.* [12] prepared TiO_2/ACF by a hydrothermal method and investigated the effect of TiO_2 loading on the photocatalytic activity of the catalyst. They found that the degradation rate of rhodamine B first increased and then decreased with the increase of loading, with the degradation efficiency reaching a maximum of 67.6% when the loading amount of TiO_2 was 75.1%. However, previous studies have mainly focused on the photocatalytic treatment of liquid-phase organic pollutants or the purification performance of high concentrations of gas-phase organic pollutants in static systems. Few reports have studied the regeneration performance and purification performance of materials for indoor gas organic pollutants in low concentrations.

In this work, TiO_2 was immobilised onto ACF by an impregnation–hydrothermal method. To examine the effect of the hydrothermal temperature, TiO_2/ACF composite materials were prepared at hydrothermal temperatures of 120, 150, 180, and 210°C. The morphology, structure, chemical composition, and optical absorption of the TiO_2/ACF composite materials were characterised by X-ray diffraction (XRD), Brunauer–Emmett–Teller (BET), scanning electron microscopy (SEM), X-ray photoelectron spectroscopy (XPS), and ultraviolet–visible (UV–vis) absorption spectroscopy. In addition, the adsorption and photocatalytic properties of the samples for gas-phase toluene were studied systematically based on the application of TiO_2/ACF composite materials in indoor air purification devices, and suitable operating parameters, such as illumination time, space velocity, and light intensity, were determined.

2. Experimental

2.1. Preparation of TiO_2/ACF composite materials: First, viscose-rayon based ACF with a specific surface area of 1289 m^2/g was immersed in a 6 mol/l nitric acid solution for 4 h at 100°C, second, washed with deionised water until the pH value was around 7.0, and dried at 110°C for 12 h. Finally, 4 ml of tetra-*n*-butyltitanate ($Ti(OC_4H_9)_4$) was dissolved in 20 ml of ethanol and mixed with magnetic stirring for 4 h. The pretreated ACF (0.2 g) was impregnated into the mixed solution for 30 min and then dried at room temperature. Then, the composite material was supported by bracket in a 100 ml hydrothermal synthesis reaction kettle with 40 ml of distilled water and heated at various temperatures (120, 150, 180, or 210°C) for 12 h. Finally, the obtained sample was washed with anhydrous ethanol and deionised water three times and dried at 80°C. According to the hydrothermal temperature used, the samples were named S120, S150, S180, and S210.

2.2. Characterisation: The crystal structure of the composite materials was studied using a D/max 2500PC automatic powder X-ray diffractometer. The specific surface area and pore volume of the composite materials were obtained using a Micromeritics ASAP2020 Analyzer. The morphology of the composite materials was characterised using an EVO MA 10L/S 10 SEM. UV–vis absorption spectra of the composite materials were recorded using a Hitachi UH4150 spectrophotometer. XPS analyses of the composite materials were obtained using an ESCALAB 250 spectrometer.

2.3. Experimental procedures and apparatus: The photocatalytic degradation efficiencies of gaseous toluene by the samples were investigated using a homemade photocatalytic reactor (Fig. 1). The air from an air cylinder was metered using a bubbling gas pipeline with access to a toluene solution at a constant temperature. Toluene exhaust fumes were mixed with diluted air, and then the mixed gas flowed into the photocatalytic reactor. The concentration of the mixed gas was controlled by adjusting the temperature of the water bath and the dilution gas flow. A 10 mm U-type quartz tube was used as the photocatalytic reactor. Illumination was provided by 8 W ultraviolet lamps (365 nm) and the light intensity was controlled by adjusting the number of lamps. The concentration of toluene was analysed using a gas chromatograph (SP-6800A) equipped with a flame ionisation detector. First, 0.1 g of the composite materials was loaded into a U-type tube reactor. The adsorption of toluene on the composite materials was conducted with a toluene concentration of about 800 ppm under dark conditions, and the toluene adsorption capacity of the fresh samples was measured. Second, the photocatalytic degradation experiments were conducted following illumination with ultraviolet light and introduction of regeneration air into the U-type tube reactor. Third, the toluene adsorption experiment was repeated, and the toluene adsorption capacity of the samples after the photocatalytic degradation reaction was measured. The second and the third steps were defined as one cycle. In this Letter, the stability of the composite materials was determined using five cycles.

The photocatalytic degradation efficiency of toluene (R) was calculated using the following equation

$$R = \frac{A_1}{A_0} \times 100\% \tag{1}$$

The degradation rate of toluene (V) was calculated using the following equation

$$V(\mathrm{mg/(h \cdot g)} = \frac{A_1}{t} \tag{2}$$

The degradation energy consumption (Q) was calculated using the following equation

$$Q(\mathrm{J/mg}) = \frac{E \times 3600t}{A_1 \times m} \tag{3}$$

where A_0 is the toluene adsorption capacity of the fresh samples (mg/g), A_1 is the toluene adsorption capacity of the samples after the photocatalytic degradation reaction (mg/g), t is the reaction time (h), m is the quantity of the composite materials (g), and E is the light intensity (W).

3. Results and discussion

3.1. Characterisation: Fig. 2 shows the XRD patterns of ACF and the prepared TiO_2/ACF composite materials. For ACF, the broad diffraction peak at $2\theta = 20°–30°$ and the weak diffraction peak at $2\theta = 40°–48°$ correspond to the (002) and (100) planes of carbon [13]. The diffraction peaks observed in all the composite materials at $2\theta = 25.28°$, 37.80°, 48.05°, and 53.89° correspond to the (101), (004), (200), and (105) planes of anatase TiO_2, respectively, which implies that the only crystalline phase in the composite materials is anatase. However, for samples prepared at higher hydrothermal temperatures, the diffraction peaks of anatase TiO_2 became stronger, suggesting that an increase of the hydrothermal temperature is favourable for the crystallinity of anatase TiO_2.

To further analyse the influence of the hydrothermal temperature on the formation of TiO_2 grains, the grain size and crystallinity of the TiO_2/ACF composite materials were calculated using Jade 6.0 (MDI), as shown in Table 1. The grain size of TiO_2 prepared by the hydrothermal method with ACF as a support was significantly smaller than that of commercial TiO_2, which was 20.7 nm [14]. This decreased grain size is mainly the result of the numerous micropores and large specific surface area of ACF, which inhibit

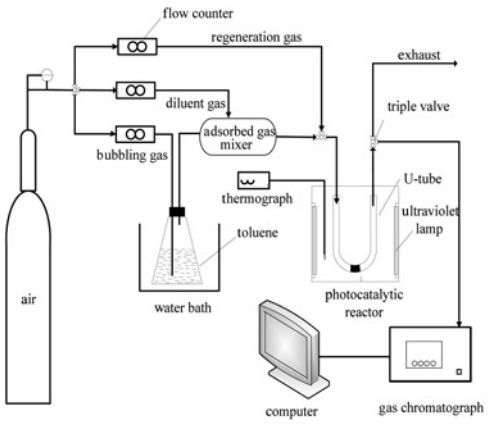

Fig. 1 *Schematic diagram of the experimental apparatus*

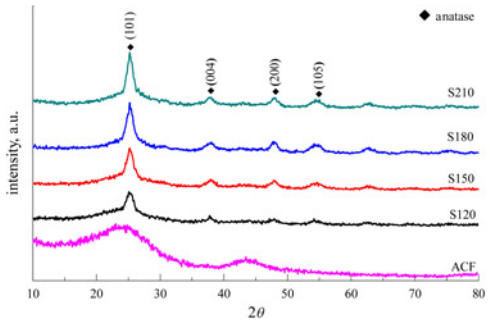

Fig. 2 *XRD patterns of ACF and the TiO_2/ACF composite materials*

doi: 10.1049/mnl.2016.0171

Table 1 Structure parameters of TiO_2/ACF composite materials

Sample	Crystalline size, nm	Crystallinity, %	Surface area, m^2/g	Total pore volume, cm^2/g	Average pore diameter, nm
S120	2.1	5.81	682.50	0.415	2.2
S150	4.1	13.60	659.07	0.409	2.3
S180	4.9	25.71	636.81	0.369	2.5
S210	6.7	25.81	567.52	0.312	2.8

the agglomeration of TiO_2 grains [15]. When the hydrothermal temperature was increased from 120 to 180°C, the grain size increased from 2.1 to 4.9 nm and the crystallinity increased from 5.81 to 25.71%. When the hydrothermal temperature was further increased to 210°C, the crystallinity increased slightly, whereas the grain size increased to 6.7 nm. This is because TiO_2 grains appear to agglomerate at the higher hydrothermal temperatures. In addition, the specific surface areas and pore volumes of the prepared composite materials are presented in Table 1. The specific surface areas of the samples were significantly smaller than that of ACF, as TiO_2 filled a portion of the pores. The specific surface areas and pore volumes showed decreasing trends with increased hydrothermal temperatures, implying that the porosity of the samples deteriorates with increasing hydrothermal temperature.

Fig. 3 displays SEM images of the TiO_2/ACF composite materials. As shown in Fig. 3*a*, in the sample prepared at the lowest hydrothermal temperature, irregular particles of TiO_2 are supported on the ACF surface. From S150 (Fig. 3*b*) to S180 (Fig. 3*c*) and to S210 (Fig. 3*d*), more and more flake TiO_2 is attached to the ACF surface. A dense and uniform TiO_2 film was formed on the surface of ACF when the hydrothermal temperature was 180°C. Moreover, when the hydrothermal temperature was further increased to 210°C, TiO_2 on the ACF surface exhibited a reunion phenomenon and the uniform film is not observed. These results indicate that the dispersion and crystallinity of TiO_2 are enhanced by increasing the hydrothermal temperature, which is consistent with the results of the XRD analysis.

Fig. 4 shows the UV–vis absorption spectra of ACF, S120, S150, S180, and S210. All the TiO_2/ACF composite materials show absorption over the entire UV–vis region. Compared with ACF, all the composite materials exhibited stronger absorption of ultraviolet light. With increasing hydrothermal temperature, the ultraviolet light absorption of the samples first increased and then decreased. The sample prepared at a hydrothermal temperature of 180°C had the highest ultraviolet light absorption. However, when the hydrothermal temperature was further increased to 210°C, the absorption of ultraviolet light by the prepared sample decreased owing to TiO_2 agglomeration on the surface of ACF, which resulted in a decrease of the surface area. These results are consistent with the results of the BET analysis.

Fig. 5 shows the curve-fitting analyses of the as-measured O1s spectra of the TiO_2/ACF composite materials. All samples showed three peaks at 530.23, 530.91, and 532.60 eV, which correspond to O–Ti bonds in the TiO_2 lattice, hydroxyl groups, and O–C bonds, respectively. It is well known that OH groups trap photogenerated holes to produce OH radicals that enhance the photocatalytic performance of TiO_2, and OH radicals also have very strong oxidising properties. The percentage of OH groups increased with increasing hydrothermal temperature (see Table 2), which implies that the photocatalytic activity is higher in samples prepared at higher hydrothermal temperatures. In addition, the percentage of O–C bonds decreased with increasing

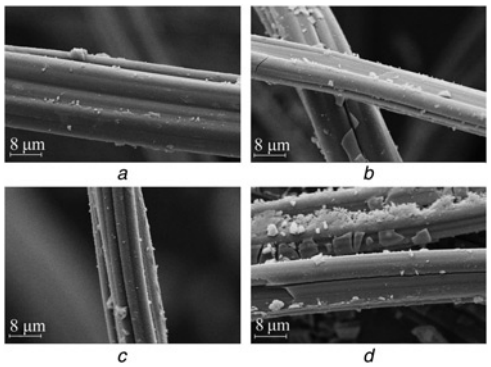

Fig. 3 *SEM images of the TiO_2/ACF composite materials (×2000)*
a S120
b S150
c S180
d S210

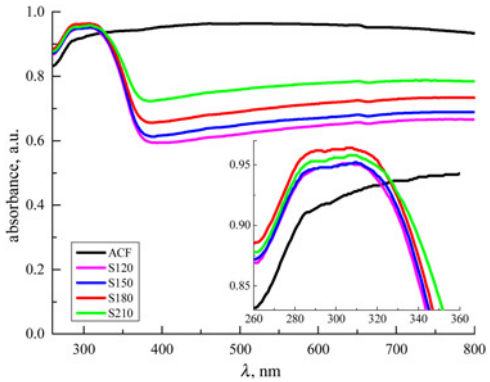

Fig. 4 *UV–vis absorption spectra of the TiO_2/ACF composite materials*

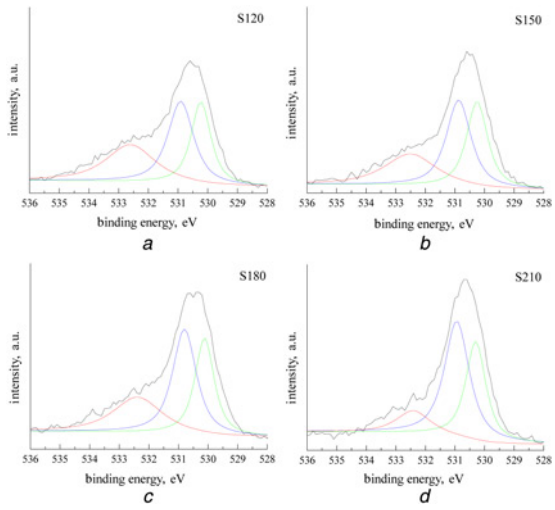

Fig. 5 *Curve-fitting analyses of the as-measured O1s spectra of the TiO_2/ACF composite materials*
a S120
b S150
c S180
d S210

Table 2 Binding energy and area ratio (%) of the characteristic peaks in the O1s spectra of the samples

Sample	O1s		
	530.23 (eV) O–Ti	530.91 (eV) O–H	532.60 (eV) O–C
S120	29.51	37.86	32.62
S150	32.59	38.14	29.27
S180	32.25	41.60	26.14
S210	32.46	44.99	22.54

hydrothermal temperature because ACF is covered with a denser TiO_2 film in samples prepared at higher hydrothermal temperatures, as demonstrated by the SEM experiments.

3.2. Effect of hydrothermal temperature on adsorption and photocatalytic degradation: The adsorption capacity and photocatalytic degradation rate of ACF and the TiO_2/ACF composite materials for toluene are shown in Fig. 6. The saturated adsorption capacities of ACF and the TiO_2/ACF composite materials prepared using different hydrothermal temperatures were about 260 and 170 mg/g, respectively. With increasing hydrothermal temperature, the adsorption capacity of the TiO_2/ACF composite materials declined slightly because the pore volume and specific surface area of the composite materials decreased with the gradual increase of the sheet structure at higher hydrothermal temperatures. During the photocatalytic degradation experiment, all the TiO_2/ACF composite materials achieved adsorption capacity regeneration, while the ACF shows unconspicuous adsorption capacity after regeneration. The results of repeated experiments show that the test error of adsorption quantity is less than 3 mg/g. For S120 and S150, the average values of adsorption capacities after regeneration were 31.92 and 35.38 mg/g, respectively. The adsorption capacity of S180 after regeneration increased a further 8.49 mg/g, whereas the adsorption capacity of S210 after regeneration decreased 5.38 mg/g. The best photocatalytic degradation efficiency of toluene was obtained for the sample prepared at a hydrothermal temperature of 180°C, and the change of degradation rate was consistent with the change of regenerative adsorption capacity. For the TiO_2/ACF composite materials, the degradation rate was mainly determined by the photocatalytic degradation ability of TiO_2 over short illumination times [16]. In combination with the results of XRD and SEM, these results indicate that the crystallinity of TiO_2 decreased when the hydrothermal temperature was 120 or 150°C.

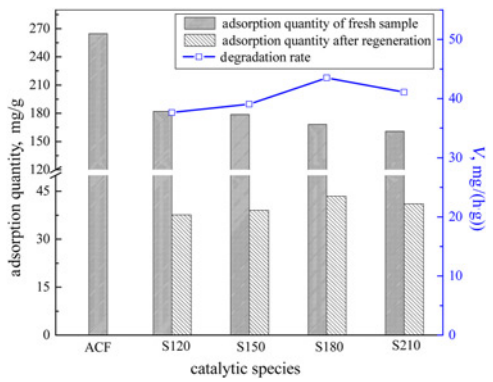

Fig. 6 *Adsorption and photocatalytic degradation properties of ACF and the TiO_2/ACF composite materials for toluene*
Reaction conditions: illumination time: 1 h, space velocity: 1400 h^{-1}, light intensity: 32 W, and reaction temperature: 20 ± *1°C*

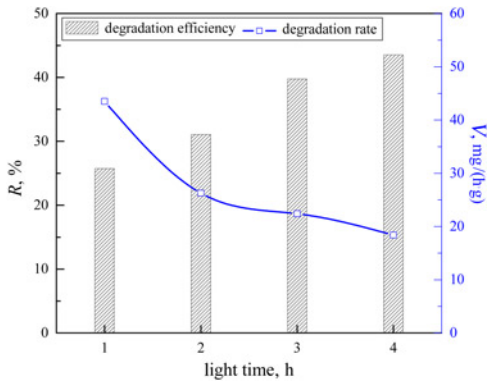

Fig. 7 *Effect of illumination time on the performance of S180 in the photocatalytic degradation of toluene*
Reaction conditions: space velocity: 1400 h^{-1}, light intensity: 32 W, and reaction temperature: 20 ± 1°C

At the same time, TiO_2 was not evenly distributed on the surface of ACF in these samples; therefore, the photocatalytic activity of the composite materials was lower. Furthermore, the crystallinity of TiO_2 in S210 slightly increased compared with that in S180, but the grain size increased significantly and TiO_2 exhibited a reunion phenomenon; therefore, the photocatalytic degradation performance of S210 decreased.

3.3. Effect of illumination time on photocatalytic degradation: Fig. 7 shows the degradation data of adsorption-saturated TiO_2/ACF for toluene under different illumination times. As shown in Fig. 7, the photocatalytic efficiency of S180 was lowest at an illumination time of 1 h, with a degradation efficiency of 25.74% and degradation rate of 43.51 mg/(h·g). With this short illumination time, the degradation efficiency is dependent on the photocatalytic degradation of toluene adsorbed on the ACF surface because the in situ photocatalytic reaction of toluene adsorbed in the micropores of ACF is not complete. As the illumination time increased, the degradation efficiency of toluene increased continuously, mainly because toluene adsorbed in the micropores of ACF was desorbed owing to the difference in the concentration of toluene between the holes and surface, and then degraded on the surface of TiO_2. Obviously, S180 exhibited excellent photocatalytic properties when the illumination time was 3 or 4 h. However, the degradation rate decreased at longer illumination times. Therefore, take the degradation rate and the degradation efficiency into consideration, it can be deduced that illumination time of 3 h gave the best photocatalytic regeneration result.

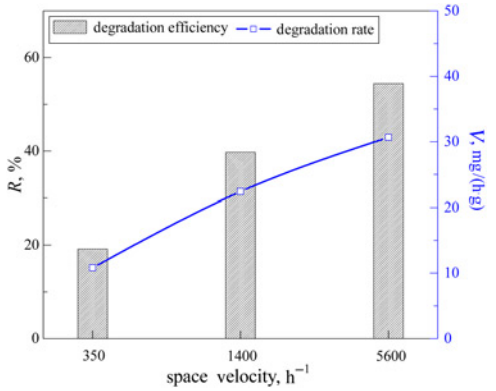

Fig. 8 *Effect of space velocity on the performance of S180 in the photocatalytic degradation of toluene*
Reaction conditions: illumination time: 3 h, light intensity: 32 W, and reaction temperature: 20 ± 1 °C

doi: 10.1049/mnl.2016.0171

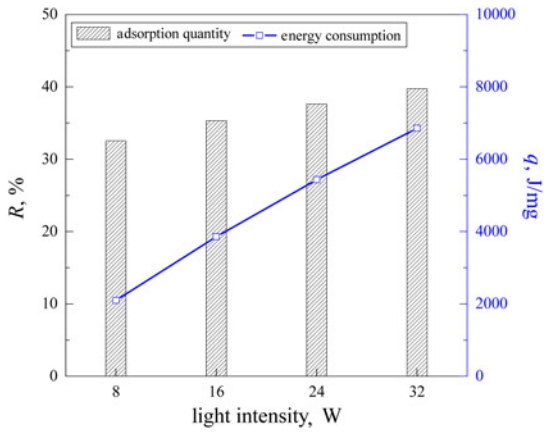

Fig. 9 *Effect of light intensity on the performance of S180 in the photocatalytic degradation of toluene*
Reaction conditions: illumination time: 3 h, space velocity: 1400 h^{-1}, and reaction temperature: 20 ± 1°C

3.4. Effect of space velocity on photocatalytic degradation: Fig. 8 shows the degradation data of adsorption-saturated TiO_2/ACF for toluene under different space velocities. When the space velocity was 350 h^{-1}, the degradation efficiency and degradation rate of toluene were only 20.81% and 10.81 mg/(h·g), respectively. A space velocity of 350 h^{-1} was unable to provide enough oxygen atoms for the photocatalytic process, as O_2 effectively improves the photocatalytic activity by trapping electrons through the formation of O^- and inhibiting the recombination of electrons and holes. The degradation efficiency and degradation rate of toluene increased when the space velocity was increased to 1400 and 5600 h^{-1} owing to sufficient oxygen atoms for the photocatalytic reaction and an improved desorption rate of toluene from the micropores of ACF.

3.5. Effect of light intensity on photocatalytic degradation: The degradation data of adsorption-saturated TiO_2/ACF for toluene under different light intensities are shown in Fig. 9. The degradation efficiency of toluene increased with increasing light intensity, which is not only attributable to an increase of the number of electrons and holes on the sample surface, but also to an improved toluene desorption rate owing to an increase of the difference in the toluene concentration between the surface and holes. However, the light intensity increase led to a reduction of energy utilisation. The degradation efficiency increased by 7.2% when the light intensity increased from 8 to 32 W, but the energy consumption increased three-fold. Based on energy consumption, which is an important consideration for household indoor air cleaners, the light intensity should not be too high.

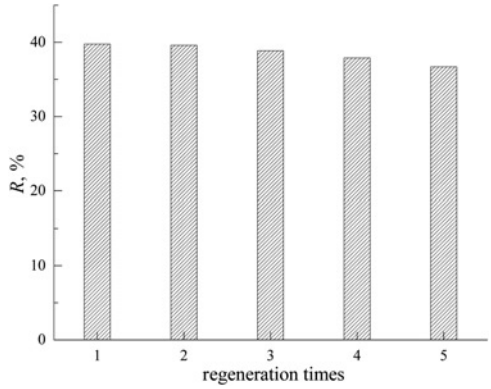

Fig. 10 *Photocatalytic stability of S180 for the photocatalytic degradation of toluene*
Reaction conditions: illumination time: 3 h, space velocity: 1400 h^{-1}, light intensity: 32 W, and reaction temperature: 20 ± 1 °C

3.6. Photocatalytic stability of TiO_2/ACF composite materials: To investigate the photocatalytic stability of S180, five recycling experiments for the photocatalytic degradation of toluene were carried out, and the results are shown in Fig. 10. The degradation efficiency of toluene was 36.7% after five cycles, which was a decrease of only 3.3% compared with the first degradation experiment. This result indicates that the sample has good regeneration performance. The decrease in photocatalytic efficiency was probably due to the absorption of an intermediate product of the degradation of toluene on the surface of the sample, which would occupy some of the active sites of the sample.

4. Conclusion: In this work, TiO_2/ACF composite materials were prepared by an impregnation–hydrothermal method. The results show that the grain size of TiO_2 was very small and TiO_2 was highly dispersed on the ACF surface. Moreover, the composite materials exhibited excellent adsorption and photodegradation properties. The hydrothermal temperature influenced the microstructure and photodegradation properties of the TiO_2/ACF composite materials, and the degradation efficiency of toluene was greatest for the sample prepared at a hydrothermal temperature of 180°C. Increasing the illumination time, space velocity, and light intensity were beneficial for regeneration of the composite materials. However, the energy efficiency decreased as the light intensity increased. In addition, the photocatalytic ability of the TiO_2/ACF composite materials did not show significant loss after reuse for five cycles. Therefore, this Letter provides a theoretical basis for the development and application of TiO_2/ACF composite materials in the field of indoor air purification.

5. Acknowledgment: This work was supported by the Project of Science and Technology Plan of Qingdao Development Zone (2014-1-35).

6 References

[1] Sun L., Li G.Y., Wan S.G., *ET AL.*: 'Mechanistic study and mutagenicity assessment of intermediates in photocatalytic degradation of gaseous toluene', *Chemosphere*, 2010, **78**, (3), pp. 313–318
[2] Poulios I., Micropoulou E., Panou R., *ET AL.*: 'Photooxidation of eosin *Y* in the presence of semiconducting oxide', *Appl. Catal. B*, 2003, **41**, (4), pp. 345–355
[3] Hashimoto K., Irie H., Fujishima A.: 'TiO_2 photocatalysis: a historical overview and future prospects', *Jpn. J. Appl. Phys*, 2005, **44**, (6), pp. 8269–8285
[4] Naoko T.I., Tsukasa T., Hiroshi Y.: 'Influence of carbon black as an adsorbent used in TiO_2 photocatalyst films on photodegradation behaviors of propyzamide', *J. Catal.*, 1998, **177**, (2), pp. 240–246
[5] Wang Y.P., Peng P.Y., Ding H.Y., *ET AL.*: 'Preparation and catalytic activity of active-carbon-supported TiO_2', *Acta Sci. Circum.*, 2005, **25**, (5), pp. 611–617
[6] Yuan R.S., Guan R.B., Zheng J.T.: 'Effect of the pore size of TiO_2-loaded activated carbon fiber on its photocatalytic activity', *Scr. Mater.*, 2005, **52**, (12), pp. 1329–1334
[7] Guo Y.H.: 'Photocatalytic degradation of phenol in wastewater over titania supported on activated carbon', *Ind. Catal.*, 2006, **14**, (6), pp. 42–45
[8] Wu Y.B., Yan Y.C., Lou T., *ET AL.*: 'The preparation of PAN composite TiO_2 nano-ACF and the conditions study', *Adv. Mater. Res.*, 2012, **586**, pp. 58–63
[9] Zhong L.X., Lee C.S., Haghighat F.: 'Adsorption performance of titanium dioxide (TiO_2) coated air filters for volatile organic compound', *J. Hazard. Mater.*, 2012, **243**, (4), pp. 340–349
[10] Shi J.W., Cui H.J., Chen J.W., *ET AL.*: 'TiO_2/activated carbon fibers photocatalyst: effects of coating procedures on the microstructure, adhesion property, and photocatalytic ability', *J. Colloid Interface Sci.*, 2012, **388**, (1), pp. 201–208

[11] Wang Y., Chen G.H., Shen Q.H., *ET AL.*: 'Hydrothermal synthesis and photocatalytic activity of combination of flowerlike TiO_2 and activated carbon fibers', *Mater. Lett.*, 2014, **116**, (2), pp. 27–30
[12] Meng H., Hou W., Xu X.X., *ET AL.*: 'TiO_2-loaded activated carbon fiber: hydrothermal synthesis, adsorption properties and photocatalytic activity under visible light irradiation', *Particuology*, 2014, **14**, (3), pp. 38–43
[13] Wang Z.H., Chen Y., Zhou C., *ET AL.*: 'Decomposition of hydrogen iodide via wood-based activated carbon catalysts for hydrogen production', *Int. J. Hydrog. Energy*, 2011, **36**, (1), pp. 216–223
[14] Le H.A., Linh L.T., Chin S.M.: 'Photocatalytic degradation of methylene blue by a combination of TiO_2-anatase and coconut shell activated carbon', *Powder Technol.*, 2012, **225**, (7), pp. 167–175
[15] Chen Y.J., Hu Z.H., Wang X.J.: 'Influence of pore size and surface area of activated carbon on the performance of TiO_2/AC photocatalyst', *Acta Phys. Sin.*, 2008, **24**, (9), pp. 1589–1596
[16] Liu S.X., Chen G.S., Sun C.L.: 'Mechanism for the photocatalytic regeneration of exhausted activated carbon', *Environ. Chem.*, 2005, **24**, (4), pp. 405–408

doi: 10.1049/mnl.2016.0171